Journal of High School Science

Altitude-dependent performance analysis of bell, aerospike and Expansion-Deflection nozzles for Rotating Detonation Engines

Hu R

Submitted: November 2, 2025, Revised: version 1, December 14, 2025, version 2, December 17, 2025
Accepted: December 18, 2025

Abstract

A Rotating Detonation Engine (RDE) is a promising alternative to traditional combustion engines found on rockets and aircraft. Conventional combustion engines rely on deflagration, or subsonic combustion, whereas RDEs utilize detonation, where the combustion front propagates at supersonic velocities. RDEs offer increased theoretical efficiency compared to conventional combustion engines, which are plateauing in terms of performance improvements. Because of this, RDE technology could significantly impact the aeronautical, astronautical, and defense industries once fully mature. Despite the growing interest in RDEs, research and analysis on the influence of nozzle geometries on RDE performance across varying pressures is still limited. This study addressed this gap by evaluating three nozzle designs–a conventional bell nozzle, aerospike nozzle, and expansion-deflection (ED) nozzle–at pressures ranging from sea level (101 kPa) to near-vacuum conditions. The ED nozzle was hypothesized to perform best relative to the ideal across the entire pressure range. Nozzle performance metrics were obtained from 2D Computational Fluid Dynamics (CFD) simulations using averaged detonation conditions. Results showed that design pressure exerted a much greater impact on performance than geometry. At low altitudes, the aerospike and bell optimized for 50 kPa significantly outperformed the ED nozzle. At high altitudes, the ED nozzle outperformed both while maintaining operability at sea level without destructive flow separation. These findings suggest that experimental designs such as the aerospike and expansion-deflection could boost RDE performance for certain operating pressure regimes and that further optimization of RDE nozzles could enhance the viability of RDE-powered launch systems.

Keywords

Aerospace engineering, Rotating Detonation Engine, Nozzle comparison, Altitude compensation, Rocket propulsion, Bell nozzle, Aerospike nozzle, Expansion-Deflection nozzle, Computational Fluid Dynamics, Thrust coefficient, Specific impulse, Supersonic flow

Roland Hu, Glenbrook South High School, 4000 W. Lake Ave. Glenview, IL 60025, USA. rhu2718@gmail.com

https://doi.org/10.64336/001c.154674

1. Introduction

Combustion engines are the basis of modern propulsion systems, powering everything from automobiles and power generators to rockets and aircraft. While these conventional combustion engines have been refined for decades, their efficiency is limited by the deflagration cycle they utilize. Detonation engines such as the Rotating Detonation Engine (RDE) offer the potential to surpass these limitations. This paper examined how nozzle design impacts RDE performance for rocket uses across the entire flight regime.

Conventional combustion engines, including rocket and air-breathing engines, are approaching their theoretical efficiency limit (1-3). These engines rely on deflagration-based combustion in which the flame front of the burning propellant propagates at subsonic velocities. In these engines, propellant (fuel and oxidizer) is compressed, combusted via deflagration, and allowed to expand through a nozzle. This process utilized by conventional combustion engines is termed the Brayton cycle (1, 3, 4), a thermodynamic model which can be used to calculate the maximum efficiency, defined as the ratio between work output and energy input. Modern combustion engines are approaching this thermodynamic efficiency limit, with further development yielding diminished efficiency gains.

In contrast to the Brayton cycle, the Humphrey cycle uses detonation-based combustion, where the combustion flame front of the burning propellant propagates at supersonic velocities (1, 4). This detonation wave causes a sharp pressure rise in a near-constant volume. This results in higher work output and therefore increased thermodynamic efficiency (~20% gain) compared to deflagration-based combustion (5, 6). Consequently, engines that use the detonation combustion cycle are an attractive replacement for conventional deflagration-based engines.

One of the most promising detonation engines under development is the RDE. In a typical RDE, propellant is injected into an annular (ring shaped) combustion chamber, where a detonation wave continuously progresses around. Due to its supersonic propagation, the detonation wave is led by a shockwave, which auto-compresses the propellant before the following combustion front ignites it to convert chemical energy into kinetic energy more efficiently than a subsonic deflagration would (1, 5). However, despite the theoretical efficiency gains, extracting maximal thrust and efficiency from the exhaust is still significantly influenced by, and dependent on, nozzle design (7).

Engine nozzles must be optimized to expand and accelerate exhaust, and engines operating within the atmosphere must be capable of operating at varying pressures. The standard nozzle used in the majority of rockets is the convergent-divergent, or bell nozzle for its performance and relative simplicity. These nozzles feature a narrow throat section to accelerate subsonic exhaust to sonic choked flow before expanding into the distinctive bell shape, accelerating the exhaust past supersonic speeds. However, these nozzles can only be optimized to provide the ideal thrust at a single ambient pressure; their design is unable to compensate for the changing

atmospheric pressures during the ascent of a rocket, providing subpar performance for the majority of the flight regime.

In contrast, an aerospike nozzle is an altitude-compensating design that retains efficient expansion of exhaust over a broad range of ambient pressures. In an aerospike, exhaust expands inwards against a central spike, similar to the expansion of the bell nozzle above. However, the aerospike does not feature an outer wall; instead, exhaust is allowed to expand outwards naturally based on pressure conditions, thus self-adjusting the effective area ratio (8). At high pressures, exhaust is forced close to the spike, recovering thrust through the increased pressure on the spike.

An expansion-deflection (ED) nozzle is also an altitude-compensating design which uses the same principle as the aerospike. The ED nozzle directs exhaust outward toward an outer wall via a central pintle, while ambient pressure forms the effective inner wall, similar to a reversed aerospike. At high ambient pressures, the engine operates in open wake mode, where the exhaust is forced close to the outside wall by a central recirculation zone, preventing overexpansion and flow separation (9). At low ambient pressures, the engine is in closed wake mode, where the exhaust can expand more freely, approximating a bell nozzle (9, 10).

While these two altitude-compensating designs offer significant advantages compared to the standard bell nozzle, they do have the disadvantage of added weight and complexity through their additional cooling needs while also requiring an additional central body to be suspended aft of the combustion chamber (8). However, the annular RDE engine geometry favors the addition of these altitude-compensating designs since the combustion chamber already provides the central body, potentially further increasing performance compared to conventional rocket engines (7, 11). Nonetheless, due to the experimental geometry and unsteady detonation flow properties of an RDE, nozzle design and optimization remains immature.

1.1 Summary

This paper examined the use of bell, aerospike, and ED geometries for an RDE nozzle across a spectrum of ambient pressures. The aim was to compare different nozzle designs across pressures ranging from sea level (101 kPa) to near vacuum—representative of a rocket's entire flight envelope—to determine an optimal nozzle geometry for a future RDE-powered launch vehicle. We hypothesized that the expansion-deflection nozzle would provide optimal performance throughout the majority of the flight envelope, matching the bell and aerospike designs at high pressures and outperforming them at low pressures. To evaluate the performance of each design, Computational Fluid Dynamics (CFD) software with inflow conditions from high-thrust NASA testing was used. The results showed that design pressure exerted a stronger influence on performance than geometry. The aerospike and bell nozzle demonstrated similar performance trends, while the ED nozzle performed comparatively poorly at low altitudes but excelled at high altitudes. Unlike the aerospike, the ED nozzle's altitude-compensation was demonstrated, exhibiting the theorized open

wake and avoiding destructive flow separation at low altitudes seen in bell nozzles of similar exit ratio. These results demonstrated the viability of these experimental nozzle designs for an RDE. The aerospike may be best suited for the booster stage of an RDE-powered rocket, due to it providing greater thrust at sea level, while the ED nozzle may be best suited for a future single-state-to-orbit (SSTO) vehicle, optimized for low pressures while still maintaining operability at sea level. This is a step in realizing the full performance benefits of an RDE, revolutionizing air and space travel with increased payload and reduced fuel consumption.

2. Methods

This study examined the performance differences of nozzle designs at various altitudes. The key design and operating parameters including combustor conditions, exhaust properties, and nozzle geometry were obtained from experimental NASA data, software simulations, and fundamental flow equations. The nozzle performance data was obtained from CFD software with analysis consisting of performance charts, contour visualization, as well as comparison with other sources.

2.1 Objectives

The objective of this study was to compare the performance of RDE nozzles across a range of pressures. Multiple nozzle geometries with varying parameters were tested using 2D CFD simulations. Engine thrust with each design was compared from sea level (101 kPa) to near-vacuum conditions. This pressure range represented the environment an RDE-powered rocket would encounter during ascent. For operating conditions representative of real use, the combustion chamber design and parameters were based on the 2023 NASA Marshall RDE test campaign (12).

To reduce computational time while still maintaining reasonable accuracy, the detonation process and resultant pressure fluctuations were not directly simulated. Instead, the time-averaged exhaust conditions were used for the 2D simulation. As found by Harroun (7), the use of 2D time averaged conditions in place of full 3D detonation waves did not significantly affect the accuracy of simulated nozzle performance.

2.2 Engine parameters

2.2.1 *Combustor geometry*

The annular combustion chamber dimensions were modeled after the NASA Marshall RDE test campaign. The inner body of the RDE had a diameter of 5.59 in. with a 0.33 in. wide annular gap forming the combustion chamber (12). Since detonation waves were not simulated and only the averaged exit pressure was required for the 2D case, the full combustor length was not necessary. Instead, post-detonation exhaust was fed through a 0.5 in. section of chamber immediately upstream of the nozzle.

2.2.2 *Combustor operating conditions*

The NASA Marshall RDE test campaign included a single high-pressure, high-thrust test representative of real use. For this test, gaseous oxygen (O_2) and methane (CH_4) were used as oxidizer and fuel at a 3.74 O/F mixture ratio (oxidizer and fuel mass ratio). The highest mean chamber pressure achieved (stagnation

pressure) was 4.29 MPa with a total mass flow of 7.39 kg/s (12). Static pressure at the combustor exit was not directly reported but was required as a boundary condition for CFD simulations. It was therefore calculated using the ideal isentropic relations (13, 14).

$$\dot{m} = AP_0M\sqrt{\frac{\gamma}{RT_0}\left(1+\frac{\gamma-1}{2}M^2\right)^{-\frac{\gamma+1}{\gamma-1}}} \quad \text{Eq. 1}$$

$$\frac{P}{P_0} = \left(1+\frac{\gamma-1}{2}M^2\right)^{-\frac{\gamma}{\gamma-1}} \quad \text{Eq. 2}$$

Solving these relations with the exhaust properties defined in the next section resulted in a Mach number of 1.59 at the combustor exit–a reasonable supersonic estimate (4, 7)–and a static pressure of 1.10 MPa. These operating conditions were used for all nozzle simulations (Table 1).

Table 1. Summary of combustor conditions. Conditions were derived from NASA RDE testing data or calculated from the data.

Parameter	**Value**
Fuel	gaseous methane (CH_4)
Oxidizer	gaseous oxygen (O_2)
Mixture ratio (O/F)	3.74
Stagnation pressure	4.29 MPa
Static pressure at combustor exit	1.10 MPa
Total mass flow rate	7.39 kg/s
Mach number at combustor exit	1.59

2.2.3 *Exhaust properties*

The simulation used averaged post-detonation exhaust gases instead of simulating the full detonation process itself, the latter requiring complex calculations and hence being resource intensive. Using the Chemical Equilibrium with Applications (CEA) program developed by NASA (15), these post-detonation exhaust gas properties were obtained from the combustion chamber conditions defined earlier. The exhaust was assumed frozen, where no additional reactions occured after initial combustion. The relevant properties extracted from NASA CEA were as follows: total temperature, 3562 K; molar mass of exhaust, 22.03 g/mol; specific heat capacity at constant pressure c_p, 2191 J/(kg·K), and the ratio of specific heats γ, 1.21 (Table 2).

Table 2. Exhaust gas properties for all nozzle simulations. Properties derived from combustor conditions using Chemical Equilibrium Analysis.

Property	Value
Total temperature	3562 K
Molar mass	22.03 g/mol
c_p	2191 J/(kg·K)
γ	1.21

2.3 Nozzle design

Three different nozzle designs suited to the unique annular geometry of an RDE were selected to test: a bell nozzle, similar to the bell nozzles found on conventional rockets but with a short central spike to ensure smooth expansion across the inner combustor body; a flared aerospike nozzle; and an ED nozzle. The bell nozzle profile was chosen as a baseline comparison, since it is used on all operational launch vehicles today but lacks altitude compensation. The aerospike and ED nozzle were chosen for their altitude-compensating abilities, which theoretically allow for similar or increased performance compared to the bell nozzle at various altitudes.

2.3.1 *Bell*

Since exhaust flow from an RDE combustion chamber is already supersonic, only a diverging section was used. This section expands the supersonic flow, increasing its velocity while decreasing the pressure. The flow was assumed isentropic, where the flow is smooth such that no dissipative effects, including turbulence or heat transfer, occur. For this diverging nozzle, the area ratio between the exit and throat determined the exit Mach number and pressure, which were needed for optimal design. The isentropic equation relating the area ratio to the ratio of specific heats γ and the Mach number is shown below (14).

$$\frac{A}{A^*} = \frac{1}{M}\left[\frac{2+(\gamma-1)M^2}{\gamma+1}\right]^{\frac{\gamma+1}{2(\gamma-1)}} \quad \text{Eq. 3}$$

(Eq 3) relates the area A and Mach number M anywhere in the nozzle to the area A* of the throat, where it was assumed that M = 1. However, M > 1 at the throat for this RDE. Applying (eq 3) to both the nozzle exit and RDE throat yields the following equation.

$$\frac{A_e}{A_t} = \frac{M_t}{M_e}\left[\frac{2+(\gamma-1)M_e^2}{2+(\gamma-1)M_t^2}\right]^{\frac{\gamma+1}{2(\gamma-1)}} \quad \text{Eq. 4}$$

(Eq 4) relates the area ratio between the exit and throat to their respective Mach numbers. A design exit pressure of 50 kPa was selected, representative of typical first-stage rocket engines. Using (eq 4), this corresponded to an area ratio of 8.06 relative to the combustor throat

and an exit radius of 3.97 in. This nozzle served as the performance baseline for comparison with altitude-compensating designs (Figure 1a).

2.3.2 *Aerospike*

A flared aerospike was used to ensure proper expansion in the limited combustor diameter (Figure 1b). The design pressure of the aerospike was 50 kPa to ensure equal comparison against the bell nozzle. The same isentropic equations outlined above also applied to this case; hence, the exit area and expansion ratio were the same as that of the bell. However, due to the limited diameter of the combustor, the spike could not be designed optimally, which affected the altitude compensation ability.

2.3.3 *Expansion-Deflection*

The ED nozzle was designed for optimal open wake performance at 50 kPa with the exit area ratio at the pintle base plane being the same as that of the bell and aerospike. After transitioning to closed wake, exhaust spreads across the entire outer nozzle, and the exit area of the outer nozzle was designed to provide the optimal expansion ratio at 10 kPa. In an optimal ED nozzle, exhaust is directed at an angle towards the outside walls; however, the supersonic nature of the RDE exhaust inhibits this turning towards the outside, since the resulting shock losses greatly reduce performance. A preliminary simulation demonstrated that even with shallow pintle angles (10º), supersonic shock losses appeared, and wake closure was not significantly affected. Hence, the pintle was designed parallel with the combustion chamber while only the outer walls expanded, achieving only a slight outwards turning of the flow (Figure 1c).

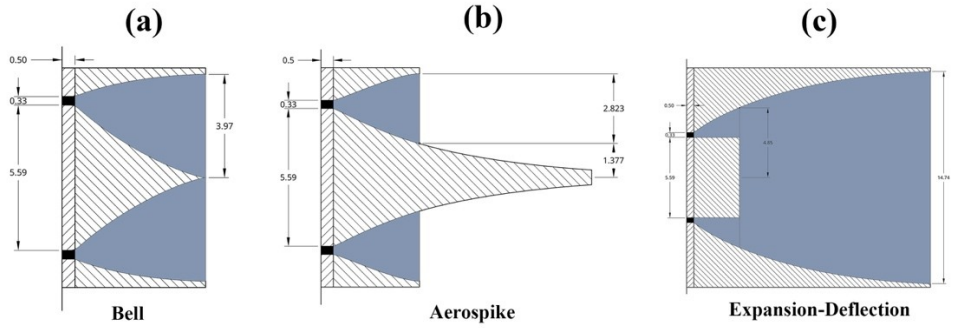

Figure 1. Geometry and dimensions of the three different RDE nozzles. a) bell nozzle **b)** flared aerospike nozzle **c)** expansion-deflection nozzle. Each nozzle was designed to provide optimal expansion at 50 kPa ambient pressure, except for the expansion-deflection nozzle which was designed for 50 kPa optimal expansion under open wake mode and 10 kPa optimal expansion under closed wake mode. RDE exhaust gas was fed through the short 0.5" combustor exit shaded black before reaching the nozzle.

2.4 Computational setup

All simulations were performed in Ansys® Fluent (16), a commercial CFD solver using a 2D axisymmetric case to reduce computing time while still maintaining accuracy. A quadrilateral mesh was employed with mesh refinement near the engine throat and nozzle to better capture the shocks, wall interactions, and turbulent

recirculation zones. The bell nozzle was composed of 89267 mesh elements, the aerospike of 100236 elements, and the ED nozzle of 126814 elements. The combustor exit was modeled as a mass flow inlet with static pressure, total temperature, and mass flow rate defined according to the properties above. Ambient pressure was varied across four values to capture pressures from sea-level to high atmosphere, near vacuum conditions: 101 kPa (sea level), 50 kPa, 10 kPa, and 1 kPa (near vacuum). The nozzle walls were modeled as being adiabatic, where no heat transfer occurred. For the simulation boundaries, a pressure far-field at the ambient conditions was employed. The symmetry centerline was specified as an axis (Figure 2).

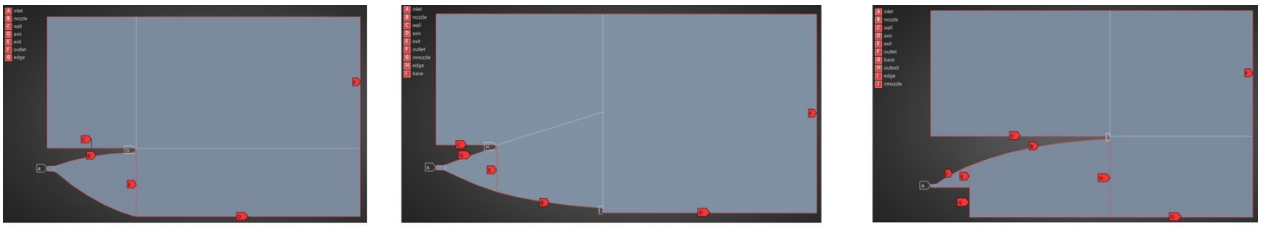

(a) bell domain (b) aerospike domain (c) expansion-deflection domain

Figure 2. Computational fluid dynamics simulation domain and boundaries in Ansys® Fluent. a) bell nozzle domain **b)** flared aerospike nozzle domain **c)** expansion-deflection nozzle domain. A 2D axis-symmetric simulation case was set up to save computing time while maintaining accuracy. Each simulation domain was set up with appropriate boundary conditions. A quadrilateral mesh was generated with local mesh refinement near the inlet and nozzle walls to accurately capture flow phenomena.

The density-based solver in Fluent® was used for the compressible flow. The exhaust was modeled as an ideal gas with properties from CEA defined above. The SST k-ω turbulence model was applied to accurately simulate turbulent effects, such as the turbulent recirculation zone near the base of the ED nozzle, or any potential flow separation. All simulations were run in double precision. Convergence was defined as residuals falling below 1×10^{-4} for continuity, momentum, and energy.

Each simulation followed an identical workflow using the Ansys® Workbench Fluent workflow: CAD import; mesh generation with quadrilaterals and local refinement; simulation setup with parameters specified above, and default parameters otherwise; solving; and post-processing of results using Fluent's integral reporting tools and contour visualization.

All simulations were performed using Ansys® Fluent 2025 Student R1 on a Lenovo Ideapad 5 laptop with an Intel® Core™ Ultra 5 Processor 225U (12 cores, 14 threads, base speed 1.5 GHz, up to 4.8 GHz maximum). Only 4 of the 12 cores were used due to limitations of the student software.

2.5 Performance metrics

There are various ways to characterize nozzle performance, including total thrust, specific impulse (I_{sp}), and thrust coefficient (C_f). Specific impulse is a measure of efficiency, defined as $I_{sp}=\frac{F}{\dot{m}g_0}$ where F is the total thrust, ṁ is the mass flow rate and g_0 is the standard gravitational acceleration, 9.81 m/s^2. Similarly, the thrust coefficient is defined as $C_f=\frac{F}{p_0 A_t}$ where p_0 is the stagnation pressure and A_t is the throat area. However, for this study, ṁ, g_0, p_0, and A_t were constant across all simulation cases; hence, the relative variation of these metrics depended solely on the total thrust. Therefore, only total thrust was required to characterize the nozzle performance in this study.

For the bell nozzle, thrust is split into two contributions: momentum thrust and pressure thrust. The total thrust is the sum of these contributions (9) as given by eq. 5. For the aerospike, total thrust is the sum of the momentum thrust, pressure thrust, and net force due to pressure on the spike surface (17), given by eq. 6.

$$F_{bell} = \dot{m}v_e + (p_e - p_a)A_e \quad \text{Eq. 5}$$

$$F_{ae} = \dot{m}v_e + (p_e - p_a)A_e + \int_S (p - p_a)\boldsymbol{n} \cdot d\boldsymbol{s} \quad \text{Eq. 6}$$

The last term is the surface integral giving the axial force due to pressure on the spike. **n** is the unit vector in the axial direction, and **s** is the surface normal (17). The dot product sums only the axial contributions.

The ED nozzle is similar to the aerospike, except that the surface integral is applied over the nozzle downstream of the exit and includes an additional term representing the thrust contribution from the pintle.

$$F_{ed} = \dot{m}v_e + (p_e - p_a)A_e + \int_S (p - p_a)\boldsymbol{n} \cdot d\boldsymbol{s} + (p_p - p_a)A_p \quad \text{Eqn. 7}$$

For an ED nozzle with a closed wake, the thrust may also be calculated in the same manner as the bell nozzle, with the exit taken at the very end of the nozzle; both these methods were utilized, and both yielded the same result.

For comparison against an ideal nozzle at all ambient pressure conditions, the ideal thrust for the RDE exhaust properties and dimensions defined in Tables 4 and 5 were calculated using the isentropic flow equations—at an ambient pressure of 101325 Pa, the ideal thrust was 20148 N; at 50000 Pa, the ideal thrust was 21384 N; at 10000 Pa, the ideal thrust was 23523 N; and at 1000 Pa, the ideal thrust was 25530 N. The altitude compensation ability of a particular nozzle was indicated by comparing the percentage of ideal thrust (the ratio between simulated thrust and ideal thrust) at each altitude.

Table 3. Ideal engine thrust at the given pressures. Isentropic flow equations were used to calculate the ideal thrust based on combustor conditions and exhaust properties.

Ambient Pressure [Pa]	Ideal Thrust [N]
101325	20148
50000	21384
10000	23523
1000	25530

2.6 Validation and uncertainty quantification

Experiments were carefully designed to ensure the validity of simulation results. First, a mesh independence study was performed by refining the mesh for each geometry up to ~250k elements and performing a simulation at a pressure of 50 kPa. The changes in calculated thrust between the refined mesh and the original mesh were less than 0.3% for all geometries, implying that the solutions to these nozzles were relatively mesh-independent. For turbulence modeling, a representative study of the ED nozzle at 10 kPa was performed due to its turbulent zone near the base. The turbulence model was changed to k-ε and Spalart-Allmaras, keeping all the other parameters the same. For both models, there was no significant observed difference in the plume, and the change in calculated thrust was 0.9%. To assess boundary condition uncertainty, the inlet static pressure was perturbed by ~ 5%. The resulting change in thrust was 1% due to contrasting changes in momentum and pressure thrust. The mass flow rate was a constant known variable, and based on literature (17), small fluctuations up to 1.5% have been observed. However, the changes in thrust averaged to zero, hence uncertainty in mass flow rate was not evaluated. A solver sensitivity study was performed on a representative bell nozzle case at 50 kPa by varying solver settings, including varying residual targets and discretization order. Across these settings, the change in calculated thrust remained below 0.2% indicating that solution sensitivity to solver configuration was insignificant. For geometry sensitivity, the unconstrained geometry (throat-nozzle wall angle and nozzle length) were modified by ~ 10%. Thrust changed by a maximum of 0.4%. This insignificant sensitivity was expected because thrust in fixed-area nozzles is governed primarily by chamber pressure, throat area, and exit area, while contour details have minor influence as long as the flow remains attached and shock-free. This indicated that the theoretical nozzle was geometrically robust. Finally, the bell nozzle case was repeated 3 times to assess variability between each run. There was almost no difference in calculated thrust (<0.1%), hence a statistical assessment of replicates was deemed unnecessary. The total uncertainty in the calculated thrust (and by extension, C_f and I_{sp}) were estimated by adding the individual uncertainties above in quadrature, yielding a total uncertainty of 1.5%. Assuming these uncertainties were independent and approximately normally distributed, the 95% confidence interval corresponded to ~ ±3.0%.

Comparison of the bell nozzle at sea level against experimental testing supported the physical plausibility of the results. The combustor exhaust properties and geometry were based on the 4171 lbf (pound-force) NASA Marshall RDE test, which also used a similar nozzle geometry (12). Qualitatively, the simulated plume exhibited similar features to the 4171 lbf test, notably slight overexpansion and shock diamonds forming immediately aft of the central tip (12). Remarkably, the simulated bell nozzle thrust at sea level in this study differed by ~3%. While this is not indicative of the true accuracy of simulations - since exact nozzle dimensions were not matched - it strongly supports the physical plausibility of the results. Furthermore, the calculated thrust coefficient for the aerospike nozzle was consistent with aerospike testing results by Harroun (7), further supporting the validity of results.

3. Results

To evaluate how nozzle geometry affected RDE performance across a rocket's ascent profile, the three designs - bell, aerospike, and ED - were tested in CFD simulations at four ambient pressures: 101 kPa, 50 kPa, 10 kPa, and 1 kPa. These pressures represented conditions from sea level to near-vacuum. Realistic combustor operating conditions were derived from NASA RDE testing, with the exhaust properties obtained from chemical equilibrium software. Each nozzle was designed according to mathematical predictions of the supersonic exhaust.

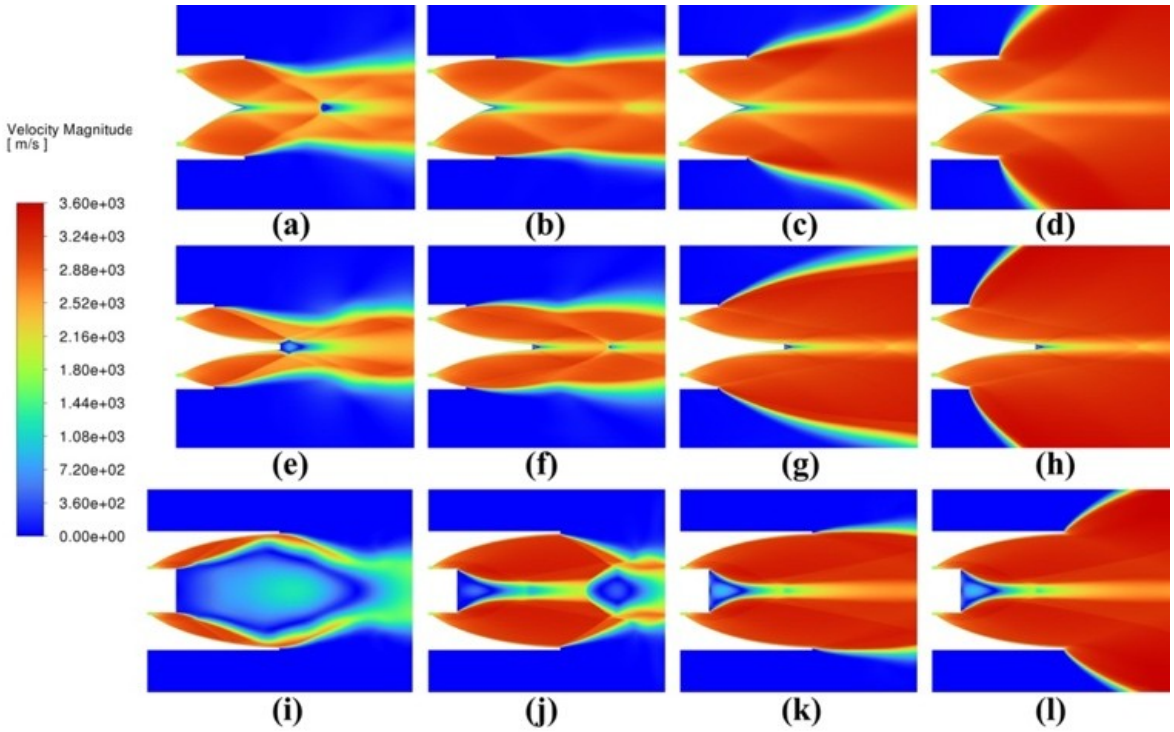

Figure 3. Velocity contours of the RDE nozzle exhaust plumes. Panels show simulated exhaust plumes for the three nozzle types—bell **(a-d)**, aerospike **(e-h)**, expansion-deflection **(i-l)**—at pressures of 101325 Pa **(a, e, i)**, 50000 Pa **(b, f, j)**, 10000 Pa **(c, g, k)**, and 1000 Pa **(d, h, l)**. Colors represent velocity magnitude.

3.1 Bell nozzle

The bell nozzle served as a baseline for comparison due to its widespread use in conventional rocket engines. Evaluating its performance under varying pressures established a reference point to compare against the experimental aerospike and ED nozzle designs. Designed for an exit pressure of 50 kPa, CFD analysis found an actual area-averaged exit pressure of 59 kPa, higher than expected. This discrepancy was attributed to slight flow separation on the central cone, which reduced the effective exit area.

At 101 kPa, there was noticeable over-expansion of the exhaust; the exit pressure was lower than ambient pressure, causing the exhaust plume to compress immediately behind the nozzle (Figure 3a). This lower exit pressure than the ambient pressure caused a negative pressure thrust, resulting in a backwards force of 1351 N on the engine, thus reducing total thrust (Table 4). At 50 kPa, near optimal expansion occurred as expected from its design, indicated by the mostly straight plume behind the nozzle (Figure 3b). The ambient pressure was ~ equal to the exit pressure. At this point, the nozzle was the most efficient, reaching 96.9% of the ideal thrust. At the low ambient pressures of 10 kPa and 1 kPa, the plume expanded outwards past the nozzle, indicating significant underexpansion (Figure 3 (c-d)). While there was an increase in total thrust due to increased pressure thrust, the nozzle performance was comparatively worse; the percent of ideal decreased relative to the performance at 50 kPa. This occured because the reduction in ambient pressure increased the pressure thrust even when the nozzle was not optimally expanded, and the decrease in percent of ideal thrust indicated that a larger fraction of the exhaust expansion occurred outside the nozzle. The expansion outwards past the nozzle does not contribute to the thrust; a larger nozzle could have harnessed this outwards expansion, converting it into increased momentum thrust. Subsequently, the ideal performance percentage decreased to 93.5 % at 10 kPa and 87.3 % at 1 kPa (Table 4).

Table 4. Performance of the bell nozzle as a function of pressure. Total thrust is presented alongside its components (momentum and pressure thrust). Efficiency is shown as a percentage of ideal thrust for each pressure condition, as well as C_f and I_{sp}. $\dot{m}$ = 7.39 kg/s for all cases (see Table 1). Statistical variation between replicate runs was negligible (<0.1%) and is not included. Uncertainties in calculated thrust, C_f, and I_{sp} are reported based on the 95% confidence interval derived from simulation uncertainties.

Ambient Pressure [Pa]	**Momentum Thrust [N]**	**Pressure Thrust [N]**	**Total Thrust [N]**	**% of ideal**	**C_f**	**I_{sp} [s]**
101325	20428	-1351	19077±572	94.7%	1.12±0.03	263±7
50000	20456	262	20718±622	96.9%	1.22±0.04	286±9
10000	20463	1537	22000±660	93.5%	1.30±0.04	303±9
1000	20463	1825	22288±669	87.3%	1.31±0.04	307±9

3.2 Aerospike nozzle

The aerospike nozzle was of particular interest because it was designed to provide altitude compensation, potentially maintaining high efficiency across a wide pressure range. The area-averaged exit pressure of the aerospike was 54 kPa, 4 kPa higher than its design pressure. The effective expansion ratio was thus marginally higher than the bell, resulting in slightly higher momentum thrust (Table 5).

At sea level (101 kPa), the aerospike was noticeably over-expanded, similar to the bell nozzle, and the plume compressed against the spike (Figure 3e). Like the bell, there was a large negative thrust contribution; this was unexpected, as the compression of the plume against the spike should have reduced this effect, compensating for the higher ambient pressure with a greater pressure thrust. At 50 kPa, the plume was predominently straight, with only slight overexpansion due to the small 4 kPa pressure difference at the exit (Figure 3f). At this point, the nozzle achieved its optimal performance at 98% of the ideal, 1.4% better than the bell. At 10 kPa, the plume was under-expanded similar to the bell (Figure 3f); however, its ideal performance percentage decreased by 2.8%, compared to the 3.4% drop of the bell, indicating some altitude compensation (Table 5). Finally, at 1 kPa, significant under-expansion was visible (Figure 3g). At this point, the thrust increase was negligible, and performance dropped further.

Table 5. Performance of the aerospike nozzle as a function of pressure. Total thrust is presented alongside its components (momentum thrust, pressure thrust, and spike thrust), with efficiency shown as a percentage of ideal thrust for each pressure condition, as well as C_f and I_{sp}. $\dot{m}$ = 7.39 kg/s for all cases (see Table 1). Statistical variation between replicate runs was negligible (<0.1%) and is not included. Uncertainties in calculated thrust, C_f, and I_{sp} are reported based on the 95% confidence interval derived from simulation uncertainties.

Ambient Pressure [Pa]	Momentum Thrust [N]	Pressure Thrust [N]	Spike Thrust [N]	Total Thrust [N]	% of ideal	C_f	I_{sp} [s]
101325	20779	-1508	-69	19202±576	95.3%	1.13±0.03	265±8
50000	20791	119	114	21024±631	98.3%	1.24±0.04	290±9
10000	20793	1395	266	22454±674	95.5%	1.32±0.04	310±9
1000	20793	1682	300	22755±683	89.2%	1.34±0.04	314±9

3.3 Expansion-Deflection nozzle

The expansion–deflection (ED) nozzle was tested as an alternative altitude-compensating design to the aerospike. One of the main features of the ED nozzle was its dual mode operation: open wake mode at high ambient pressures (design exit pressure of 50 kPa) and closed wake mode at low ambient pressures (design exit pressure of 10 kPa). However, simulations showed premature wake closure at 50 kPa, reducing expected performance (Figure 3j).

At sea level (101 kPa), the ED nozzle created a large recirculation zone in the center, keeping

flow attached to the nozzle walls and preventing separation (Figure 3i). However, the average pressure in this circulation zone was almost half that of the ambient pressure, at 56 kPa from CFD analysis. This large low pressure region combined with the large exit area created a strong negative pressure thrust, significantly decreasing performance to 73.6% of ideal (Table 6). At 50 kPa, the nozzle transitioned to an over-expanded closed wake, with exhaust flowing out of almost the entire exit area. Two recirculation zones formed; one near the pintle, and one after the exit (Figure 3j). The negative pressure thrust became less severe, and performance reached 87.3% of ideal, still significantly worse than the bell and aerospike. At 10 kPa, the nozzle was at optimal performance, with a straight exhaust plume (Figure 3k). Here, the ED nozzle outperformed both the aerospike and bell, reaching 98% of ideal thrust. At 1 kPa, the exhaust was grossly underexpanded (Figure 3l), and performance dropped to 94.2% of ideal (Table 6).

Table 6. Performance of the expansion-deflection nozzle as a function of pressure. Total thrust is presented alongside its components (momentum thrust, pressure thrust, nozzle thrust, and base thrust), with efficiency shown as a percentage of ideal thrust for each pressure condition, as well as C_f and I_{sp}. $\dot{m}$ = 7.39 kg/s for all cases (see Table 1). Statistical variation between replicate runs was negligible (<0.1%) and is not included. Uncertainties in calculated thrust, C_f, and I_{sp} are reported based on the 95% confidence interval derived from simulation uncertainties.

Ambient Pressure [Pa]	**Momentum Thrust [N]**	**Pressure Thrust [N]**	**Nozzle Thrust [N]**	**Base Thrust [N]**	**Total [N]**	**% of ideal**	**C_f**	**I_{sp} [s]**
101325	20029	-1419	-3026	-748	14836±445	73.6%	0.87±0.03	204±6
50000	20030	217	-872	-703	18672±560	87.3%	1.10±0.03	257±8
10000	20030	1494	1611	-87	23048±691	98.0%	1.36±0.04	318±10
1000	20030	1781	2171	56	24038±721	94.2%	1.42±0.04	332±10

3.4 Comparison

The bell and aerospike reached their best performance near 50 kPa, achieving 96.9% and 98.3% of ideal thrust, respectively. Both experienced efficiency losses at higher and lower pressures, with the aerospike offering negligible improvement in altitude compensation relative to the bell. In contrast, the ED nozzle performed poorly at 101 kPa and 50 kPa, dropping to 73.6% and 87.3% of ideal thrust, respectively, but reached 98.0% of ideal thrust at 10 kPa, outperforming both the bell and aerospike at this pressure (Figure 4a). Also, the performance decrease for the ED nozzle between 10 kPa and 1 kPa was less than that of the bell and aerospike, at a 3.8% decrease compared to a 6.3% and 6.2% decrease from the aerospike and bell, respectively (Figure 4b).

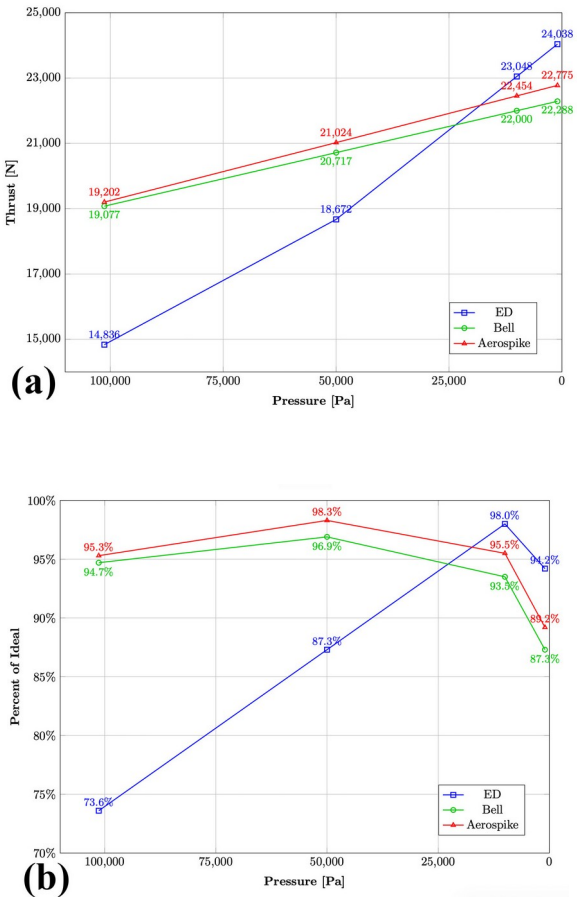

Figure 4. Performance of three different RDE nozzle types across a range of ambient pressures. The effects of ambient pressure on **(a)** the thrust and **(b)** the percentage of ideal thrust. Thrust was obtained from CFD simulations, while ideal thrust was calculated with isentropic flow equations. The smooth trends reflect interpolation between points; however, a finer pressure sweep may reveal differences in the trends, particularly for the ED nozzle near wake transition.

4. Discussion

The results of this study suggest that both the bell and aerospike nozzles are optimal for high-mid ambient pressure conditions, while the ED nozzle offers an efficient near-vacuum solution that is still operable at sea level. The bell and aerospike nozzles achieved peak efficiencies at 50 kPa, with the aerospike slightly outperforming the bell. However, contrary to expectations, the aerospike did not demonstrate significant altitude compensation. Its performance closely followed that of the bell nozzle across all pressures. Due to the constraint on dimensions imposed by the RDE combustor, the aerospike could not demonstrate altitude compensation as theorized. The limited combustor geometry may have constrained the spike size and expansion ratio, reducing its effectiveness.

The aerospike and bell both reached approximately equal peak efficiencies at 50 kPa and both underwent ~ equal performance decreases at other pressures. In contrast, the ED nozzle reached its highest efficiency at 10 kPa. Although its performance at higher ambient pressures (101 kPa and 50 kPa) was significantly lower—73.6% and 87.3% of ideal, respectively—it maintained flow attachment at these high ambient pressures despite performing best at 10 kPa. This is particularly notable because a bell nozzle optimized for the same low pressures would typically experience destructive flow separation at sea level, causing damaging structural oscillations (10). The ED nozzle's open wake mode at high ambient pressures, facilitated through its central recirculation zone, prevented such separation, allowing it to remain operable across the wide pressure range.

These findings suggest that nozzle geometry alone does not guarantee top performance at a particular ambient pressure; instead, the design exit pressure has a greater impact on performance at a particular altitude than geometry. Furthermore, the lack of altitude compensation produced by the aerospike as well as the greater than expected losses of the ED nozzle at ≥ 50 kPa demonstrate the challenges of nozzle integration with a pre-existing RDE combustion chamber. The spike size of the aerospike was limited by the diameter of the combustor. With an optimal, larger spike, the overexpansion and negative pressure thrust at sea level could have been compensated for with a large forward spike thrust. These integration challenges are consistent with findings by Harroun (7). For the ED nozzle, the lack of significant outward turning of the flow by the pintle resulted in premature closing of the wake and reduced nozzle thrust, reducing its low altitude performance. The supersonic nature of the RDE exhaust inhibits this necessary outwards turning, as turning the supersonic flow would cause large unwanted shock losses. The reduced altitude compensation of a shallow angle ED nozzle for conventional rockets is supported by Schomberg et al. (11). Additionally, premature wake closure could be mitigated through base-bleed injection. However, this mechanism was not incorporated into the present simulations due to complexity and solver instability issues. The reduced low-altitude performance observed for the ED nozzle is therefore consistent with the absence of these control strategies, and future RDE ED designs would likely require either bleed or active pintle control to realize the full theoretical altitude-compensating behavior. All these findings demonstrate the importance of taking into consideration the desired nozzle and altitude performance when designing an RDE combustor. For a future RDE-powered launch vehicle, having appropriate combustor dimensions to accommodate an efficient nozzle is critical.

The results are limited by several simplifying assumptions, including a 2D axisymmetric domain, time-averaged inflow in place of the inherently unsteady RDE exhaust, frozen chemistry, an ideal-gas model, and adiabatic walls. Literature suggests that steady inflow and 2D approximations introduce thrust overestimates on the order of a few percent for attached flows (7, 12). However, the ED nozzle may experience larger overestimates of up to

10% because of its large recirculation zone, which is not fully captured by steady or axisymmetric assumptions (7). Further combustion of exhaust products in the nozzle can also shift thrust predictions by up to 6%, increasing thrust compared to frozen chemistry (18). A representative comparison using a real-gas model showed a 1–2% decrease in thrust relative to the ideal gas model, and a fixed-wall-temperature test indicated that wall heat transfer effects contributed ~ a 1% decrease. Since these effects represent modeling errors rather than statistical uncertainty, they are not combined into a single total uncertainty; instead, they indicate the expected magnitude of deviation introduced by the physical assumptions, and should not significantly affect the comparative trends between nozzle geometries. Additionally, the large underestimate caused by the frozen chemistry assumption and the various smaller overestimates from the other assumptions appear to partially cancel out, which may partially explain the 3% difference in performance relative to real NASA testing.

This study indicates that achieving high RDE performance is less about adopting a specific nozzle geometry and more about ensuring that the nozzle is properly matched to the combustor and the intended ambient pressures. Development should focus on integrated combustor–nozzle systems rather than relying on theoretical altitude-compensating designs alone. An integrated design would allow a greater portion of the available exhaust at high altitudes to be converted into thrust rather than wasted expanding outside the nozzle. Even though thrust already increases with altitude in this study, integrated designs would allow for further increases and a higher percentage of ideal, enabling better-performing and more efficient RDE-powered launch vehicles in the future. Future research should include a high-definition 3D transient simulation of the fluctuating RDE exhaust flow to capture the potentially unexpected flow properties unable to be determined by a 2D simulation, as well as explore base bleed affects for the ED nozzle to prevent premature wake closure. In addition, the many assumptions can be fully simulated with more complex and higher fidelity work, such as thermal modeling. Finally, experimental validation of nozzle and combustor designs at altitude should be incorporated and compared with CFD results.

5. Conclusion

RDEs could revolutionize space travel with higher combustion efficiencies. However, optimal nozzle design is required to realize the benefits. Current RDE nozzle studies mostly focus on aerospike geometries at standard atmospheric pressure, neglecting lower ambient pressures. This study compared bell, aerospike, and expansion-deflection geometries across pressures ranging from 101 kPa (sea level) to 1 kPa (near-vacuum) using realistic launch vehicle combustor conditions.

The results suggested that nozzle performance was strongly dictated by the optimal design pressure, with geometry having only secondary effects. The bell and aerospike nozzle both achieved ~ equal performance. However, the ED nozzle stood out as exhibiting stable performance despite being optimized for a low ambient pressure; aerospike and bell geometries optimized to the same pressure would

experience destructive flow separation at sea level. The findings also demonstrated that successful RDE design should consider combustor dimensions based on desired nozzle geometry and performance, as the limited combustor dimensions nullified the aerospike's theorized altitude compensation and led to premature wake closure in the ED nozzle. Fixed combustor designs combined with the limitations of supersonic exhaust inhibit the potential advantages of aerospike and ED nozzles.

RDE technology is maturing, and optimal nozzle design and integration is one of the important research areas necessary to realize the benefits of this next-generation propulsion system for aerospace and defense.

6. References

1. Zhou, R., Wu, D., Wang, J. (2016). "Progress of Continuously Rotating Detonation Engines." Chinese Journal of Aeronautics, 29(1), 15–29. https://doi.org/10.1016/j.cja.2015.12.006

2. Li, Rui., Xu, J., Huang, S. (2022). "Nozzle Design for Rotating Detonation Engine." Journal of Propulsion and Power, 38(5), 849–865. https://doi.org/10.2514/1.B38539

3. Qin, X., Yang, Q., Wang, H., Xu, X., Haidn, O. (2025). "Research Progress in Rotating Detonation Propulsion Technology." Acta Astronautica, 236, 522–546. https://doi.org/10.1016/j.actaastro.2025.06.064

4. Xie, Q., Ji, Z., Wen, H., Ren, Z., Wolanski, P., Wang, B. (2020). "Review on the Rotating Detonation Engine and Its Typical Problems." Transactions on Aerospace Research, 2020, 107–167. https://doi.org/10.2478/tar-2020-0024

5. Raman, V., Prakash, S., Gamba, M. (2023). "Nonidealities in Rotating Detonation Engines." Annual Review of Fluid Mechanics, 55, 639–674. https://doi.org/10.1146/annurev-fluid-120720-032612

6. Liu, G., Wang, Z., Ruan, Y., Zhong, Z., Wang, R., Zhou, S., et al. (2025). "Experimental Study on Effects of Nozzles and Combustors on the Rotating Detonation Rocket Engine in Pulse Operation." Results in Engineering, 27, 105974. https://doi.org/10.1016/j.rineng.2025.105974

7. Harroun, A. J. (2019). "Investigation of nozzle performance for rotating detonation rocket engines." M.Sc. thesis, Purdue University, 1–113. https://hammer.purdue.edu/articles/thesis/Investigation_of_Nozzle_Performance_for_Rotating_Detonation_Rocket_Engines/8799218

8. Kumar, K. N., Gopalsamy, M., Antony, D., Krishnaraj, R., Viswanadh, C. B V. (2017). "Design and optimization of aerospike nozzle using CFD." IOP Conference Series: Materials Science and Engineering, 247, 012008. https://doi.org/10.1088/1757-899X/247/1/012008

9. Hagemann, Gerald., Immich, H., Nguyen, T. V., Dumnov, G. E. (1998). "Advanced Rocket Nozzles." Journal of Propulsion and Power, 14(5), 620–633. https://doi.org/10.2514/2.5354

10. Smalley, K. B., Brown, A., Ruf, J., Gilbert, J. "Flow Separation Side Loads Excitation of Rocket Nozzle FEM." NASA Technical Reports Server. https://ntrs.nasa.gov/api/citations/20070031864/downloads/20070031864.pdf

11. Schomberg, K., Olsen, J., Doig, G. (2015). "Analysis of a Low-Angle Annular Expander Nozzle." Shock and Vibration, 2015(1), article ID 675861. https://doi.org/10.1155/2015/675861

12. Teasley, T. W., Fedotowsky, T. M., Gradl, P. R., Austen, B. L., Heister, S. D. (2023). "Current State of NASA Continuously Rotating Detonation Cycle Engine Development." AIAA SCITECH 2023 Forum. https://doi.org/10.2514/6.2023-1873

13. "Mass flow rate equations." NASA Glenn Research Center, National Aeronautics and Space Administration, https://www1.grc.nasa.gov/beginners-guide-to-aeronautics/mass-flow-rate-equations/

14. Houghton, E. L., Carpenter, P. W., Collicott, S. H., Valentine, D. T. (2017). *Aerodynamics for Engineering Students*, 7th ed. pp. 255–327, Elsevier.

15. Gordon, S., and McBride, B. J. "Computer program for calculation of complex chemical equilibrium compositions and applications." NASA Lewis Research Center, 1996, https://ntrs.nasa.gov/api/citations/19960044559/downloads/19960044559.pdf

16. Ansys Inc. "Ansys® Student, Release 2025 R1." Ansys Inc. https://www.ansys.com/academic/students/ansys-student

17. Paxson, Daniel E., Miki, K., Perkins, H. D., Yungster, S. (2022). "Computational Fluid Dynamic Optimization of an Experimental Rotating Detonation Rocket Engine Nozzle." AIAA AVIATION Forum. https://doi.org/10.2514/6.2022-4107

18. Zhukov, Victor P. (2019). "The Impact of Methane Oxidation Kinetics on a Rocket Nozzle Flow." Acta Astronautica. 161, 524-530. https://doi.org/10.1016/j.actaastro.2019.01.001